Journal of Alloys and Compounds 509 (2011) 8487–8492

Contents lists available at ScienceDirect

Journal of Alloys and Compounds

journal homepage: www.elsevier.com/locate/jallcom

Partial inverse spinel structure of manganese-doped gahnite: XRD and EPR spectroscopy studies

J. Popović[a,*], B. Gržeta[a], B. Rakvin[b], E. Tkalčec[c], M. Vrankić[a], S. Kurajica[c]

[a] Division of Materials Physics, Ruđer Bošković Institute, Bijenička cesta 54, P.O. Box 180, HR-10002 Zagreb, Croatia
[b] Division of Physical Chemistry, Ruđer Bošković Institute, Bijenička cesta 54, P.O. Box 180, HR-10002 Zagreb, Croatia
[c] Faculty of Chemical Engineering and Technology, University of Zagreb, Marulićev trg 19, HR-10000 Zagreb, Croatia

ARTICLE INFO

Article history:
Received 6 April 2011
Received in revised form 30 May 2011
Accepted 1 June 2011
Available online 12 June 2011

Keywords:
Transition metal alloys and compounds
Sol–gel processing
Crystal structure
X-ray diffraction
Electron paramagnetic resonance

ABSTRACT

Manganese-doped $ZnAl_2O_4$ (gahnite) samples, with doping levels 0, 4.3, 7.6 and 11.7 at.% Mn (substituting for Zn), were prepared using a sol–gel technique and characterized by X-ray powder diffraction. Diffraction lines were broadened indicating on nanocrystalline samples, the line broadening depended on Mn doping level. The samples were cubic with a spinel-type structure, space group $Fd\bar{3}m$. Manganese doping of gahnite caused an increase of unit-cell parameter. The structure of the gahnite samples was refined by the Rietveld method, simultaneously with the analysis of diffraction line broadening. Valence state and the location of manganese ions in the structure were determined by EPR spectroscopy. Pure gahnite possessed the normal spinel structure, while Mn-doping induced the appearance of partial inverse spinel structure with Mn^{2+} ions residing on both tetrahedral and octahedral cation sites. Metal-oxide distances in the $(Zn,Mn,Al)O_4$ tetrahedra and $(Al,Mn)O_6$ octahedra increased as the Mn-doping level increased, resulting in the unit-cell parameter enlargement. Crystallite size decreased and lattice strain increased on the increase of Mn loading.

1. Introduction

Zinc aluminate, $ZnAl_2O_4$ (gahnite), owing to its good optical and catalytic properties, has attracted interest as a phosphor host material for applications in luminescent displays, self-diagnosis systems, mechano-optical stress sensors, and stress-imaging devices [1–4], as well as catalyst and catalyst support material [5]. When doped with Co^{2+}, Mn^{2+} or rare earth cations, gahnite exhibits luminescence and can be used as a cathodoluminescent material [6]. Since it is extremely stable, chemically and thermally, gahnite emerged as an alternative choice to sulphide-based phosphors which are known to become unstable under electron beam exposure in a 10^{-7} mbar vacuum, resulting in a chemical degradation of the phosphor layer and a detrimental effect on cathodoluminescent efficiency [7,8].

Gahnite has a spinel structure, which belongs to the cubic space group $Fd\bar{3}m$ with eight formula units per unit cell, and can be described with a general formula AB_2X_4. The unit cell contains 32 oxide anions in cubic close-packed lattice (ccp). There are 64 tetrahedral interstices and 32 octahedral interstices between oxide anions in the cubic unit cell. In AB_2X_4 spinels, 8 of 64 tetrahedral interstices are occupied by A^{2+} cations, while 16 of 32 octahedral interstices are occupied by B^{3+} cations. By convention, unit-cell origin can be either on an A-site cation ($\bar{4}3m$ symmetry) or on an octahedral vacancy ($\bar{3}m$ symmetry) [9]. In literature the latter choice is used more frequently, with A^{2+} cations on Wyckoff positions 8*a* (1/8, 1/8, 1/8), B^{3+} cations on position 16*d* (1/2, 1/2, 1/2), and O^{2-} anion on position 32*e* (*u*, *u*, *u*), where the oxygen coordinate is called a parameter *u*. For a perfect ccp anion arrangement and origin at $\bar{3}m$, $u_{ideal} = 1/4$. The cation distribution where divalent cation resides on tetrahedral 8*a* site and trivalent cation on octahedral 16*d* site is referred as the "normal" spinel distribution. However, cation distribution between these two sites is influenced by (i) temperature, (ii) electrostatic contribution to the lattice energy, (iii) cationic radii, (iv) cationic charge, and (v) crystal-field effects. All the mentioned effects can cause an appearance of the "inverse" spinel structure, where A^{2+} and B^{3+} cations are not exclusively residing on tetrahedral and octahedral site, respectively. The degree of cation disorder is described by an inversion parameter, δ [10]. This parameter is defined as a fraction of trivalent metal cation B^{3+} on tetrahedral cation sites, and so the general structural formula for spinels can be written as $^{IV}[A_{1-\delta}B_{\delta}]\,^{VI}[B_{2-\delta}A_{\delta}]\,X_4$, where δ may have values between 0 and 1.

A detailed structural study of pure zinc aluminate (both single crystal and powder) was performed in wide temperature range (from 700 °C up to 1400 °C) by O'Neill and Dollase [11]. Unit-cell

* Corresponding author. Tel.: +385 1 4561 120; fax: +385 1 4680 114.
E-mail addresses: jpopovic@irb.hr, jpopovic@irb.hr (J. Popović).

0925-8388/$ – see front matter © 2011 Elsevier B.V. All rights reserved.
doi:10.1016/j.jallcom.2011.06.006

parameter a slightly increased in annealing as a consequence of small increase in inversion parameter δ (0.01–0.06, depending on temperature of annealing). Even a longer thermal treatment at higher temperatures did not result in any further increase of δ. The maximum value of inversion parameter for gahnite, achieved at annealing temperature of 1400 °C, was only 0.06. From those investigations it could be concluded that gahnite generally possesses a normal spinel structure regardless of the annealing procedure. Singh et al. [12] prepared $ZnAl_2O_4$:Mn (1 at.% Mn) by urea combustion technique involving furnace temperature of ~500 °C during a short period of time (<5 min). The EPR spectrum of thermal treated sample exhibited a resonance signal at $g \approx 2$ having a six-line hyperfine structure characteristic for Mn^{2+} ions in an axial symmetry sites. Also, a green photoluminescence peak at 511 nm was observed (with excitation of λ_{exc} = 387, 427 and 456 nm) and it was assigned to a transition from the upper $^4T_1$ to ground state $^6A_1$ of Mn^{2+} ion in tetrahedral coordination. Those EPR and photoluminescence studies led to the conclusion that manganese ions were present in divalent state and that the site symmetry around Mn^{2+} ions was distorted tetrahedral. Lou and Hao [13] prepared thin films of $ZnAl_2O_4$:Mn (2 at.% Mn) grown on aluminosilicate ceramic plates using spray pyrolysis of aqueous solutions. Cathodoluminescence properties of the films under low to medium excitation voltage (<5 kV) were investigated. The authors found green emission from samples that were annealed at temperatures above 550 °C, the emission was ascribed to Mn^{2+} ions located on the tetrahedral site of the spinel structure. Pure manganese aluminate, $MnAl_2O_4$, known by the mineral name galaxite, possesses a partial inverse spinel structure as found by Hålenius et al. [14] from XRD single crystal data. Structural formula of the sample was obtained to be $^{IV}[Mn_{0.90}Al_{0.10}]\ ^{VI}[Mn_{0.10}Al_{1.90}]\ O_4$, obviously showing the presence of Mn^{2+} ions on both cation sites, tetrahedral and octahedral, respectively, with the inversion parameter δ = 0.10.

Recently we prepared powder gahnite samples doped with 0–100 at.% Co using a sol–gel technique [15]. It was found that cobalt doping of gahnite induced the inverse spinel structure at only 4 at.% Co. Inversion parameter δ increased with the increase of Co doping level, from 0.037 for 4 at.% Co to 0.248 for 100 at.% Co. On the basis of our structural results for Co-doped gahnite [15] and cited literature data for Mn-doped gahnite [12,13] along with the crystal structure of pure $MnAl_2O_4$ [14], it is expected that Mn-doped gahnite should exhibit some level of inverse spinel structure even for the low levels of manganese doping. Elucidating the dopant ion distribution between two cation sites in the spinel structure is important, since it is a determing factor for controlling and forecasting the material properties. The present paper reports the preparation of powder Mn-doped gahnite samples, their structural characterization and size-strain analysis. The location of manganese in the gahnite structure has been proposed on the basis of EPR spectroscopy and the Rietveld structure refinement of XRD powder data.

2. Materials and methods

2.1. Sample preparation

The powder samples of pure $ZnAl_2O_4$ and ones doped with manganese in the amounts of 4.3, 7.6 and 11.7 at.% (the samples S0–S3) were prepared using a sol–gel technique followed by thermal treatment. Aluminum-*sec*-butoxide, $Al(O^sBu)_3$ (97%, Aldrich, UK), zinc nitrate hexahydrate, $Zn(NO_3)_2{\cdot}6H_2O$ (99%, Kemika, Croatia), and manganese nitrate hexahydrate, $Mn(NO_3)_2{\cdot}6H_2O$ (99%, Kemika, Croatia) were dissolved in 2-butanole, $CH_3CH_2CH(OH)CH_3$ (99%, Kemika, Croatia) by vigorous stirring. Prepared gels were dried at room temperature during few days, and obtained dry samples were subsequently grinded to fine powders. The powders were heated up to 800 °C in the furnace with static air at a heating rate of 10 °C/min and calcined at this temperature for 2 h. Afterwards they were slowly cooled to RT in the furnace. The samples were light brown colored except of pure $ZnAl_2O_4$, which was white.

Table 1
Composition of Mn-doped gahnite samples and refined values of their unit-cell parameter; space group $Fd\bar{3}m$ (2 2 7). R_p and R_{wp} are the discrepancy factors, which characterize a quality of fitting result [21].

Sample	Mn content (at.%)	R_p	R_{wp}	a (Å)
$ZnAl_2O_4$[a]	0	–	–	8.086(1)
S0	0	0.0481	0.0633	8.0854(3)
S1	4.3(2)	0.0538	0.0776	8.0905(5)
S2	7.6(4)	0.0637	0.0800	8.0918(2)
S3	11.7(6)	0.0746	0.0946	8.0931(2)

[a]Data cited from [11].

2.2. Methods

The manganese concentrations in the samples were determined by means of PIXE (Particle Induced X-ray Emission) spectroscopy, using a nuclear microprobe facility with a 3 MeV proton beam and a semiconductor Si(Li) X-ray detector [16]. The *K*-series of emitted X-ray radiation from thin powder samples was used for the analysis.

Prepared Mn-doped samples were characterized by X-ray powder diffraction at RT using a Philips MPD 1880 counter diffractometer with monochromatized Cu $K\alpha$ radiation. Two data sets were collected for each prepared sample: (i) XRD pattern of the sample mixed with silicon powder (99.999%, Koch-Light Lab. Ltd., UK) as an internal standard reference material, scanned in steps of 0.02° (2θ) in the 2θ range from 10° to 100° with a fixed counting time of 7 s, for the purpose of precise determination of unit-cell parameter, (ii) XRD pattern of the sample scanned in the 2θ range from 10° to 140°, also in steps of 0.02° (2θ) and with fixed counting time of 7 s, for the purpose of the crystal structure refinement [17] and line broadening analysis. Unit-cell parameter a of prepared samples was determined by using the UNITCELL program [18] and refined by the whole-powder-pattern fitting method using the WPPF program [19]. Crystal structure refinement and line broadening analysis were performed by the Rietveld method using the program X'Pert HighScore Plus, version 2.1 [20]. The refinements were carried out by means of a split-type pseudo-Voigt profile function and the polynomial background model. Isotropic vibration modes were assumed for all atoms. The instrumental line broadening was determined using silicon powder (99.999%, Koch-Light Lab. Ltd., UK; spherical particles with diameter of 1 μm).

The EPR spectroscopy was used for examining the manganese oxidation state and its position in the Mn-doped gahnite structure. Investigation was carried out with standard X-band EPR spectrometer (Bruker Elexsys FT/CW 580). All spectra were obtained with the magnetic field modulation amplitude of 0.3 mT at 100 kHz. The variable microwave power in the wide range (0.002–200 mW) was employed and spectra were detected at first harmonic of modulation frequency.

3. Results and discussion

3.1. XRD characterization of the samples

XRD studies indicated that all prepared samples, S0–S3, contained only a cubic gahnite phase without any additional impurity phases. Manganese content and refined unit-cell parameter a of the samples are listed in Table 1 along with the literature data for gahnite unit-cell parameter. The unit-cell parameter of gahnite increased with Mn-doping level (Fig. 1). With Mn doping, the increase of unit-cell parameter was expected considering that ionic radius of 4-coordinated Mn^{2+} (r = 0.66 Å) is larger than that of 4-coordinated Zn^{2+} (r = 0.60 Å). Besides, it is well known that in the spinel-type structure divalent cations can also be incorporated at the octahedral cation site substituting for Al^{3+}. The substitution of Mn^{2+} for octahedral Al^{3+} would also increase the unit-cell parameter since 6-coordinated Mn^{2+} (r = 0.83 Å) is larger than 6-coordinted Al^{3+} (r = 0.535 Å). Obviously, judging solely on the basis of cell increase, the manganese incorporation site in the gahnite structure could not be unambiguously determined.

3.2. EPR spectroscopy

EPR spectra of the samples S1, S2 and S3 recorded at RT are given in Fig. 2. Spectra exhibit six-line patterns around g = 2.0044, which according to Singh et al. [12] indicated on Mn^{2+} ions in an axial symmetry sites. Each spectrum contains six strong hyper-

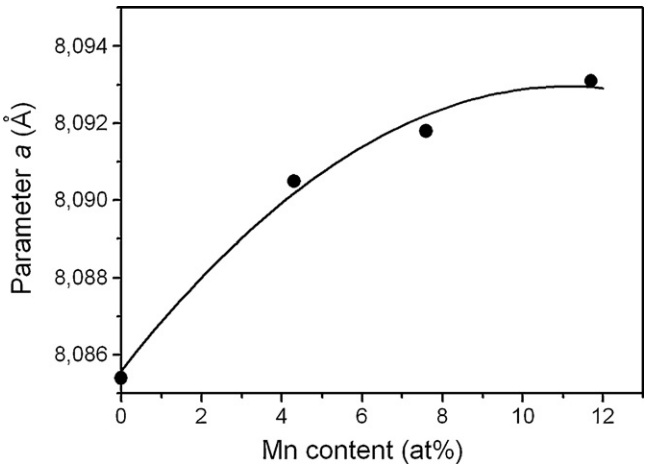

Fig. 1. Relationship between unit-cell parameter a of Mn-doped gahnite and Mn content.

fine lines ($\Delta m_S = \pm 1$, $\Delta m_I = 0$) and ten weak forbidden hyperfine lines ($\Delta m_S = \pm 1$, $\Delta m_I = \pm 1$) of Mn nucleus with $I = 5/2$ [22,23]. Forbidden lines can be seen as low intensity doublets between the main sextet lines. These doublets are more pronounced for low Mn^{2+} content. The forbidden lines in this system are expected due to mixing arising from the second order perturbation, which includes the cross product of the hyperfine coupling and the axial zero field splitting parameter D [23]. Presence of these lines indicates on some distortion that lowers the symmetry from cubic structure and supports location of the Mn^{2+} ion on octahedral site. On the other hand, for Mn^{2+} on tetrahedral site one would expect dominant contribution of symmetric sextet spectrum. In the previous studies of Mn^{2+} in similar system ($MgAl_2O_4$), it was suggested that Mn^{2+} occupies tetrahedral sites, which are slightly distorted due to the presence of forbidden transitions in the spectrum [23,24]. EPR spectra presented in Fig. 2 show rather complex composite character. In order to elucidate the composite character of the spectra, a mathematical subtraction of EPR spectrum for the lower Mn^{2+} content from the EPR spectra for higher Mn^{2+} content was undertaken. The obtained residual EPR spectra for two cases of subtraction: (a) $EPR_{(7.6\,at.\%\,Mn)} - EPR_{(4.3\,at.\%\,Mn)}$, (b) $EPR_{(11.7\,at.\%\,Mn)} - EPR_{(4.3\,at.\%\,Mn)}$, respectively, are presented in Fig. 3. Two different groups of lines can be clearly recognized in these residual spectra, as denoted by arrows (sharper and broader sextet

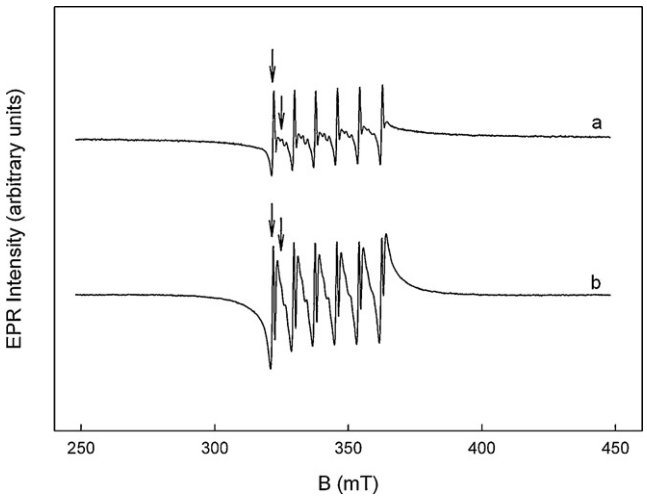

Fig. 3. Residual EPR spectra of Mn-doped gahnite: (a) $EPR_{(7.6\,at.\%\,Mn)} - EPR_{(4.3\,at.\%\,Mn)}$; and (b) $EPR_{(11.7\,at.\%\,Mn)} - EPR_{(4.3\,at.\%\,Mn)}$. The arrows denote two different groups of lines in the residual spectra: sharper and broader sextet lines, respectively.

lines). This indicates that composite EPR spectrum of Mn-doped gahnite consists of two components arising from the two different paramagnetic species. Thus, the spectral components could be related to Mn^{2+} on two different sites in the gahnite structure. Intensities of spectral components are obviously dependant on Mn^{2+} contents on these two sites.

There is a possibility that these two paramagnetic species within Mn-doped gahnite structure, giving complex composite EPR spectrum, exhibit different effective spin-lattice relaxation time, T_1. This can be checked by examination of the EPR spectrum at various microwave power intensities, P. Indeed, Fig. 4 shows different patterns of the spectra for sample S1 (4.3 at.% Mn) under the very low ($P = 0.002$ mW) and very high ($P = 200$ mW) power saturation, respectively. The effective linewidths of allowed lines of the sextet spectrum exhibit change, from $\Delta_{pp} \sim 0.8$ mT to $\Delta_{pp} \sim 1.8$ mT. This effect supports the presence of paramagnetic species with different microwave saturation behavior. The obtained spectra are scaled on the same peak-to-peak amplitude and it is noticeable that shaper sextet dominates in the composite spectrum at low microwave power, while a broader sextet dominates at high microwave power, respectively. In addition, it could be noted that forbidden lines did not show change in broadening

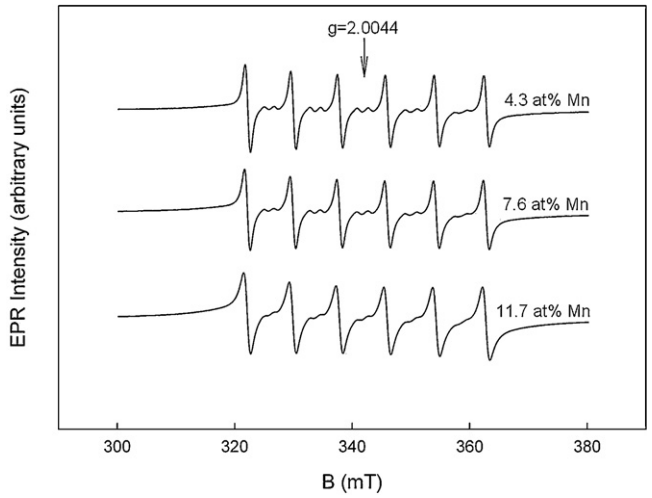

Fig. 2. EPR spectra of Mn-doped samples S1, S2 and S3 (containing 4.3, 7.6 and 11.7 at.% Mn, respectively) taken at room temperature.

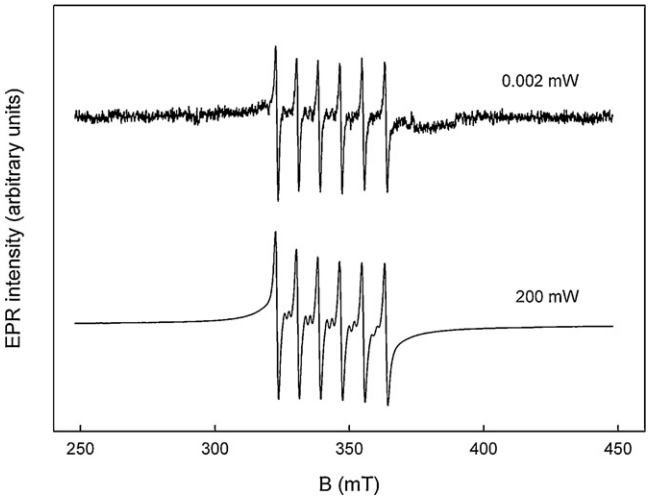

Fig. 4. EPR specta of sample S1 (4.3 at.% Mn) detected at different microwave power saturation and scaled to the same peak amplitude.

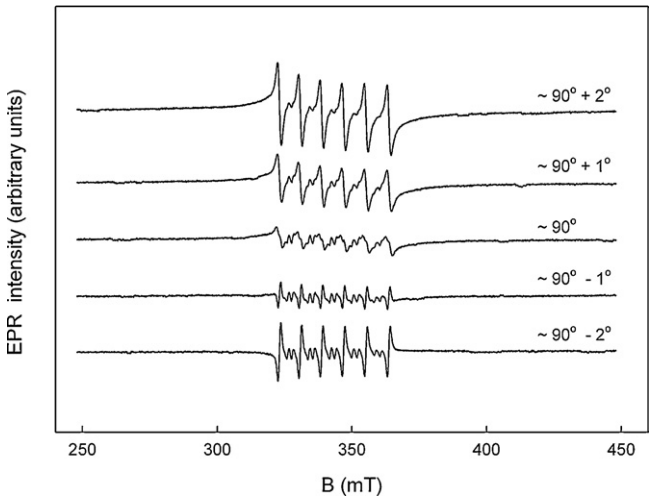

Fig. 5. EPR spectra of sample S1 detected at different modulation phase angle in the vicinity of the out of phase of modulation signal (~90°).

of effective linewidth ($\Delta_{pp,\,forb.} \sim 0.8$ mT) even at high microwave power. The obtained linewidth effect supports the evidence that forbidden lines are related to the sharper sextet component of spectra.

In order to reach possible separation between narrow and broad sextet, one expects a small difference in the phase shift for the amplitude modulation signal in the vicinity of 90° out of modulation phase. As well established in the method of transfer saturation EPR [25,26], the absorption signal detected at the first harmonic of modulation frequency (υ_M = 100 kHz) shows maximum of intensity in the phase with modulation frequency for paramagnetic species with short effective spin-lattice relaxation time ($2\pi\upsilon_M \ll 1/T_1$). The minimum of such signal, and sign change, is expected in the vicinity of 90° out of phase of the modulation frequency. Fig. 5 shows EPR spectra for sample S1 recorded by step of 1° in the vicinity of the 90° out of phase of the modulation frequency. A dominant contribution of broad sextet is detected at around 2° above the out of phase and the maximum contribution of sharp sextet (with maximum intensity of forbidden lines) is detected at 2° below the out of phase, respectively. The obtained results additionally support composite character of the EPR spectrum. It follows that the measured spectrum resulted from two paramagnetic species with different effective spin-lattice relaxation time. Thus, spectral components could be related to two possible Mn^{2+} sites. The sharp sextet with forbidden lines exhibits all characteristics which are expected for Mn^{2+} on octahedral site [23,24]. Moreover, the larger intensity ratio of forbidden lines to allowed lines, detected in this case, than the same ratio for the ordinary spectrum (in the phase spectrum) allowed more accurate evaluations of zero field splitting parameter, D. In order to calculate parameter D, the relation (1) derived by Shaffer et al. [23] was employed:

$$\frac{I_f}{I_a} = \frac{512}{15}\left(\frac{35}{4} - m^2 + m\right)\left(\frac{D}{g\mu_\beta H}\right)^2 \quad (1)$$

By employing the intensity ratio of forbidden and allowed transition (I_f/I_a = 0.203), for $m = -3/2$ and line at magnetic field of 330.8 mT, the value of D = 10.2 mT was obtained. On the other hand, intensity of forbidden lines in the broad sextet almost vanish and this spectral component could be assigned to spectrum originated from Mn^{2+} ion on tetrahedral (A) site in the gahnite structure. The above experiments support faster effective spin-lattice relaxation time and broader linewidth ($\Delta_{pp} \sim 1.8$ mT) contribution for Mn^{2+} ion on A site than for Mn^{2+} ion on B site.

The obtained spectroscopic results clearly support presence of two EPR spectral components for the Mn-doped gahnite. These spectral components are separated on the base of different effective spin-lattice relaxation time. The spectroscopic properties of these components are assigned to Mn^{2+} ion spectrum at two different sites in the gahnite lattice.

3.3. Rietveld structure refinement and analysis of diffraction line broadening

Rietveld structure refinement was performed for all prepared samples, S0–S3. The refinement for undoped gahnite (sample S0) was done using the structure of gahnite determined by O'Neill and Dollase [11] as a starting structural model. The structural model for Mn-doped samples (S1–S3) was made according to the EPR spectroscopy results. It comprised a gahnite structure in which a portion of tetrahedrally coordinated Zn^{2+} (on A site) and a portion of octahedrally coordinated Al^{3+} (on B site) were substituted by Mn^{2+}. The refinement procedure involved refinement of background parameters, zero shift, diffraction-line profile parameters, scale factor, lattice parameter a and oxygen positional parameter u. Site occupancies for cations (Zn^{2+}, Mn^{2+} and Al^{3+} on A site, and Al^{3+} and Mn^{2+} on B site) were determined indirectly, namely by varying the inversion parameter δ under the constrain that maintained the chemical composition of the samples. Isotropic temperature factors (B_{iso}) for cations sharing the same cation site were constrained to change unisonous during the Rietveld refinement.

The observed and calculated powder XRD patterns for the samples S0 and S3 are presented in Fig. 6. along with the values of full-widths at half-maximum (FWHM) in the wide range of Bragg angle. Table 2 lists refined structural parameters for samples S0–S3 and the results of line broadening analysis performed by the Rietveld refinement. Undoped sample S0 had the normal spinel structure with δ = 0, while samples S1–S3 had a nonzero inversion parameter δ which increased with the increase of Mn-doping level (Fig. 7). The oxygen positional parameter u slightly increased on

Table 2
Results of Rietveld refinements and line broadening analysis for samples S0–S3.

Sample	δ	R_{wp}	Atom site	Wyc. position	Occupancy	$x=y=z$	B_{iso}(Å^2)	Crystallite size (nm)	Lattice strain (%)
S0	0	0.059	^{IV}A	8*a*	1 Zn	0.125000	0.97(2)	18.1(1)	0.07(1)
			^{VI}B	16*d*	1 Al	0.500000	0.29(3)		
			O	32*e*	1 O	0.2644(1)	0.53(5)		
S1	0.030	0.056	^{IV}A	8*a*	0.013 Mn + 0.957 Zn + 0.03 Al	0.125000	1.13(2)	17.4(1)	0.12(1)
			^{VI}B	16*d*	0.015 Mn + 0.985 Al	0.500000	0.58(2)		
			O	32*e*	1 O	0.2645(1)	0.96(3)		
S2	0.052	0.056	^{IV}A	8*a*	0.024 Mn + 0.924 Zn + 0.052 Al	0.125000	0.67(2)	14.9(1)	0.17(1)
			^{VI}B	16*d*	0.026 Mn + 0.9740 Al	0.500000	0.41(2)		
			O	32*e*	1 O	0.2645(1)	0.63(4)		
S3	0.056	0.060	^{IV}A	8*a*	0.061 Mn + 0.883 Zn + 0.056 Al	0.125000	0.91(2)	13.5(1)	0.21(1)
			^{VI}B	16*d*	0.028 Mn + 0.972 Al	0.500000	0.52(2)		
			O	32*e*	1 O	0.2646(1)	1.14(5)		

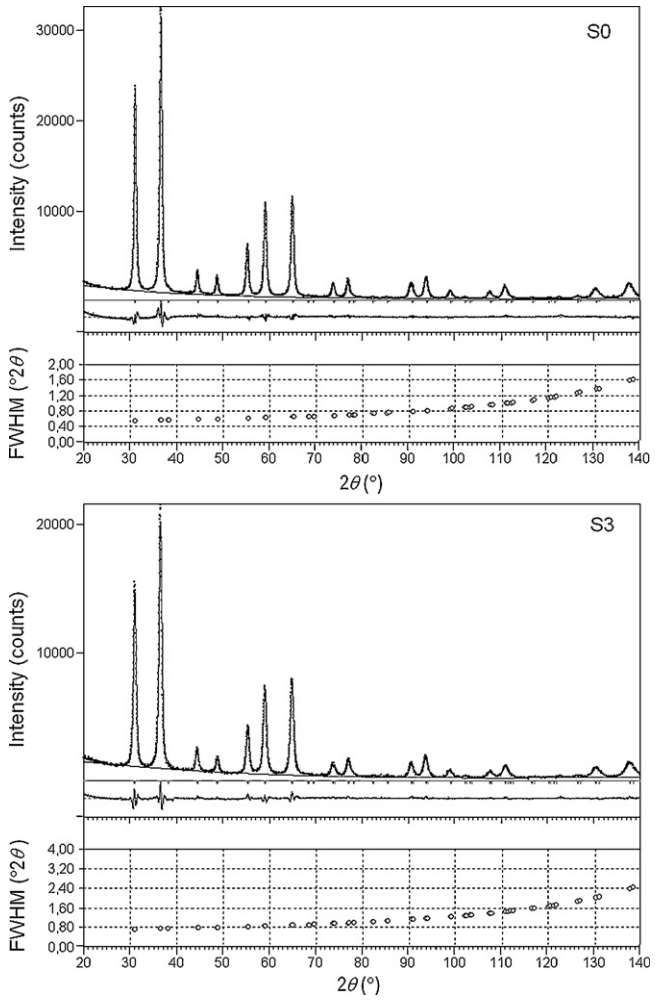

Fig. 6. Rietveld refinement and diffraction line broadening analysis for samples S0 and S3.

Mn doping, causing the slight expansion of both tetrahedral and octahedral site volume. Line broadening analysis showed that all samples were nanocrystalline. The crystallite size decreased with the increase in Mn doping level, from 18.1(1) nm for sample S0 to 13.5(1) nm for sample S3. On the other hand, the lattice strain increased with Mn doping level, from 0.07(1)% for sample S0 to 0.21(1)% for sample S3. Such behavior can be explained by the fact that introducing of dopant manganese ions into the gahnite structure causes the increase of lattice strain and disturbed the crystallites to grow.

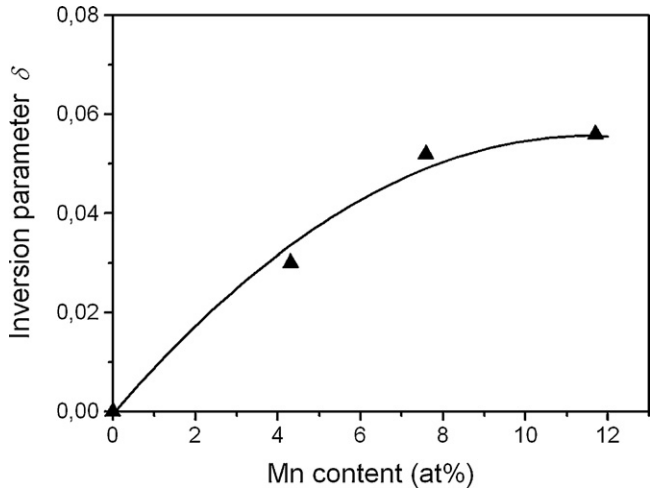

Fig. 7. Variation of inversion parameter δ with Mn content in gahnite samples.

Table 3
Metal–oxygen distances (Å) in structural tetrahedra and octahedra of gahnite samples.

Sample	Mn content (at.%)	Inversion parameter δ	Interatomic distances M–O (Å)	
			Tetrahedra	Octahedra
S0	0	0	1.953(1)	1.913(1)
S1	4.3(2)	0.030	1.955(1)	1.913(1)
S2	7.6(4)	0.052	1.956(1)	1.914(1)
S3	11.7(6)	0.056	1.957(1)	1.914(1)

Table 3 lists metal–oxygen distances in structural tetrahedra and octahedra for samples S0–S3. It is obvious that a slight expansion of structural tetrahedra and octahedra caused the expansion of unit-cell parameter of gahnite samples. The obtained cation occupancy parameters for Mn-doped gahnite showed that 3 at.% Mn occupies octahedral site and 1.3 at.% Mn occupies tetrahedral site in the sample S1. In the sample S2, 5.2 at.% Mn occupies octahedral site and 2.4 at.% Mn occupies tetrahedral site, while in the sample S3 5.6 at.% Mn occupies octahedral site and 6.1 at.% Mn occupies tetrahedral site, respectively. These data confirmed that EPR spectrum (a) shown in Fig. 3 is mainly originated from Mn^{2+} on octahedral site, while EPR spectrum (b) of the same figure is mainly originated from Mn^{2+} on tetrahedral site.

4. Conclusion

Mn-doped gahnite samples containing 0, 4.3, 7.6 and 11.7 at.% Mn were prepared by a sol–gel technique. Prepared samples were nanocrystalline. All the samples were cubic with a spinel-type structure. Unit-cell parameter a increased with the increase in Mn-doping level. Manganese ions Mn^{2+} on doping occupied both tetrahedral and octahedral cation sites of the spinel structure as evidenced by EPR spectroscopy, indicating on inducement of partial inverse spinel structure. Rietveld structure refinement revealed that structural inversion parameter δ increased with the increase of Mn content, from 0.030 for 4.3 at.% Mn to 0.056 for 11.7 at.% Mn.

Acknowledgment

Financial support from the Ministry of Science, Education and Sports of Republic of Croatia is gratefully acknowledged.

References

[1] S.K. Sampath, J.F. Cordaro, J. Am. Ceram. Soc. 81 (1998) 649–652.
[2] R. Roesky, J. Weiguny, H. Bestgen, U. Durgerdissen, Appl. Catal. A: Gen. 176 (1990) 213–220.
[3] S.K. Sampath, D.G. Kandive, R. Pandey, J. Phys.: Condens. Matter 11 (1999) 3635–3644.
[4] H. Matsui, C.N. Xu, H. Tateyama, Appl. Phys. Lett. 78 (2001) 1068–1070.
[5] R. Pandey, J.D. Gale, S.K. Sampath, J.M. Recio, J. Am. Ceram. Soc. 12 (1999) 3337–3341.
[6] G. Müller, Electroluminescence II Semiconductor and Semimetal, Academic Press, New York, 2002.
[7] J. Ballato, J.S. Lewis, P.H. Holloway, Mater. Res. Soc. Bull. 24 (1999) 51–56.
[8] H.C. Swart, T.A. Tottier, J.S. Sebastian, S.L. Jones, P.H. Holloway, J. Appl. Phys. 83 (1998) 4578–4583.
[9] K.E. Sickafus, J.M. Wills, N.W. Grimes, J. Am. Ceram. Soc. 82 (1999) 3279–3292.
[10] E.J.W. Verwey, E.L. Heilmann, J. Chem. Phys. 15 (1947) 174–180.
[11] H.St.C. O'Neill, W.A. Dollase, Phys. Chem. Miner. 20 (1994) 541–555.
[12] V. Singh, R.P.S. Chakradhar, J.L. Rao, D.-K. Kim, J. Lumin. 128 (2008) 394–402.
[13] Z. Lou, J. Hao, Appl. Phys. A 80 (2005) 151–154.
[14] U. Hålenius, F. Bosi, H. Skogby, Am. Mineral. 92 (2007) 1225–1231.
[15] J. Popović, E. Tkalčec, B. Gržeta, S. Kurajica, B. Rakvin, Am. Mineral. 94 (2009) 771–776.

[16] M. Jakšić, I. Bogdanović, D. Dujmić, S. Fazinić, T. Tadić, Strojarstvo 38 (1996) 249–254.
[17] H.M. Rietveld, J. Appl. Crystallogr. 2 (1969) 65–71.
[18] H. Toraya, J. Appl. Crystallogr. 26 (1993) 583–590.
[19] H. Toraya, J. Appl. Crystallogr. 19 (1986) 440–447.
[20] X'Pert HighScore Plus Program, version 2.1., PANalytical Almelo, Nederlands, 2004.
[21] R.A. Young, E. Prince, R.A. Sparks, J. Appl. Crystallogr. 15 (1982) 357–359.
[22] A. Abragam, B. Bleaney, Electron Paramagnetic Resonance of Transition Ions, Clarendon Press, Oxford, 1970.
[23] J.S. Shaffer, H.A. Farach, C.P. Poole Jr., Phys. Rev. B 13 (1976) 1869–1875.
[24] A. Tomita, T. Sato, K. Tanaka, Y. Kawabe, M. Shirai, K. Tanaka, E. Hanamura, J. Lumin. 109 (2004) 19–24.
[25] L.R. Dalton, B.H. Robinson, L.A. Dalton, P. Coffey, Saturation Transfer Spectroscopy. Advances in Magnetic Resonance, vol. 8, Academic Press, New York, 1976.
[26] N. Maltar-Strmecki, B. Rakvin, P. Cevc, D. Arčon, Appl. Magn. Reson. 22 (2002) 551–560.